Supplementary information

Transient metabolon dynamics tune enzyme specificity

Riki Imaizumi, Toshiyuki Waki, Yoshikazu Hattori, Kohei Takeshita, Miru Sumita, Kazutomo Kawaguchi, Hiroyuki Kumeta, Kenichi Umeda, Kyohei Sato, Taro Yanai, Hiroaki Matsuura, Takeshi Yokoyama, Risa Omura, Kayo Nakatani, Naoki Sakai, Yukimura Kawagiwa, Yamato Doi, Aoi Yasuda, Takuya Nakano, Kaichi Uno, Kunihiro Yoshida, Misato Tsunashima, Tomohide Saio, Yoshikazu Tanaka, Seiji Takahashi, Noriyuki Kodera, Kunishige Kataoka, Masaki Yamamoto, Satoshi Yamashita and Toru Nakayama

Corresponding authors: yamashita@se.kanazawa-u.ac.jp, toru.nakayama.e5@tohoku.ac.jp

Supplementary Figures

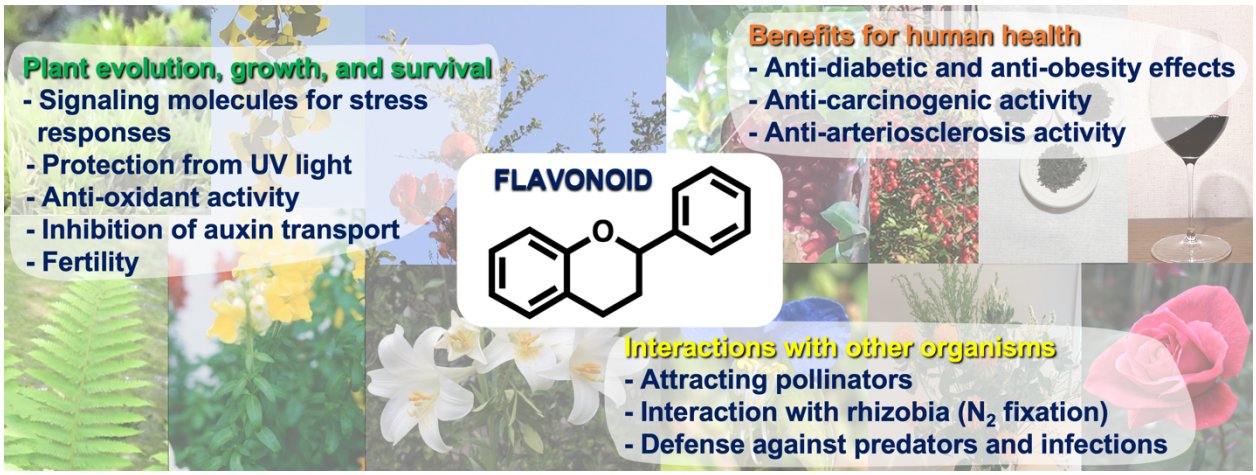

Supplementary Fig. 1. General structure of flavonoids, with the roles of flavonoids in plant growth and survival, interactions with other organisms, and health benefits in humans shown around the structure.

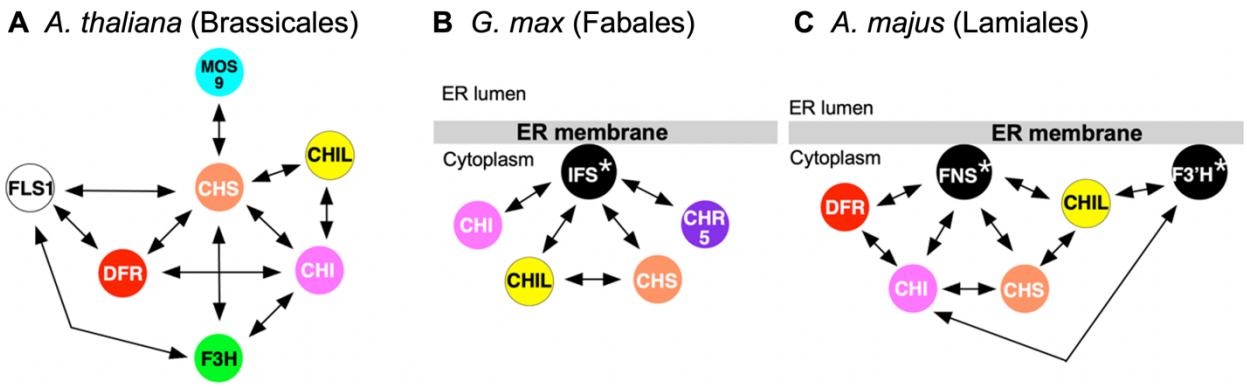

Supplementary Fig. 2. Examples of flavonoid metabolons, with identified protein–protein interactions indicated by double-headed arrows. (A) *Arabidopsis thaliana*[11,19,20,62]. (B) *Glycine max*[11,32,33]. (C) *Antirrhinum majus*[11,31]. Enzyme and protein names are as follows: CHS, chalcone synthase; CHI, chalcone isomerase; CHIL, chalcone isomerase-like protein; CHR5, chalcone reductase isozyme 5; DFR, dihydroflavonol 4-reductase; F3H, flavanone 3-hydroxyase; FLS1, flavonol synthase isozyme 1; IFS, 2-hydroxyisoflavanone synthase; F3′H, flavonoid 3′-hydroxylase; MOS9, nuclear protein associated with the epigenetic control of *R* genes that mediate effector-triggered immunity. Enzymes with an asterisk are ER membrane-bound cytochromes P450.

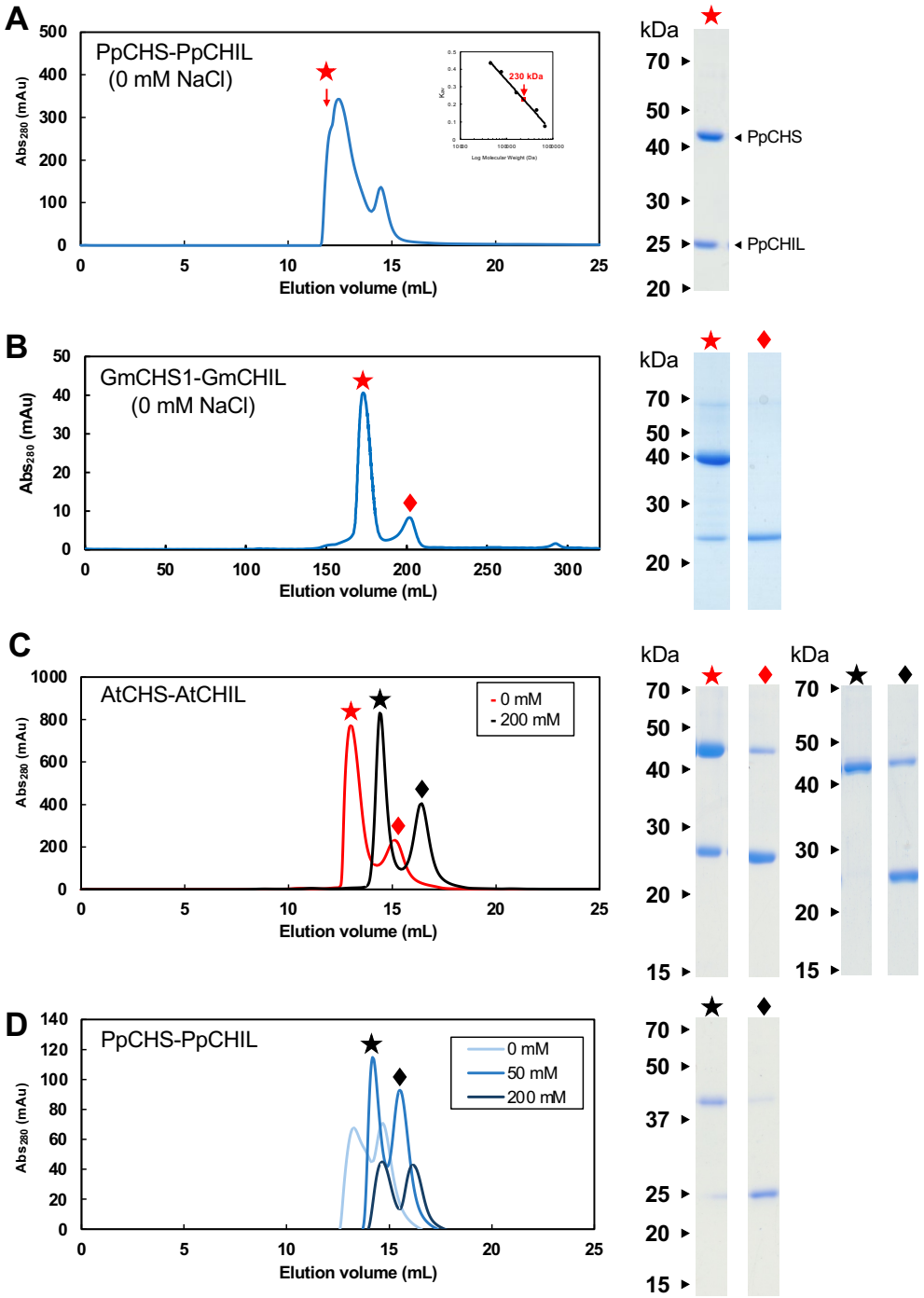

Supplementary Fig. 3. Size-exclusion chromatograms of CHS-CHIL complexes from various plants. (A) Size-exclusion chromatography of the PpCHS-PpCHIL complex. The fraction indicated by a star in the chromatogram was analyzed by SDS-PAGE (right) and used for crystallization. (B) Chromatogram of an equimolar mixture of *Glycine max* CHS and CHIL (GmCHS1 and GmCHIL, respectively) analyzed using a Hiload 26/60 Superdex 200 pg column in 50 mM Tris-HCl (pH 7.5). Symbols in the chromatogram correspond to the symbols for the SDS-PAGE results shown on the right. (C) Chromatogram of an equimolar mixture of

Supplementary Fig. 3 to be continued on the following page.

Arabidopsis thaliana CHS and CHIL (AtCHS and AtCHIL, respectively) analyzed using a Superdex 200 Increase 15/300 column in 50 mM Tris-HCl (pH 7.5) with 200 mM NaCl (black line) or without NaCl (red line). (D) Chromatogram of an equimolar mixture of PpCHS and PpCHIL analyzed using a Superdex 200 Increase 15/300 column in 50 mM Tris-HCl (pH 7.5) with 50 mM NaCl or 200 mM NaCl or without NaCl. SDS-PAGE results for the peaks under 50 mM NaCl conditions (black symbols) are shown on the right.

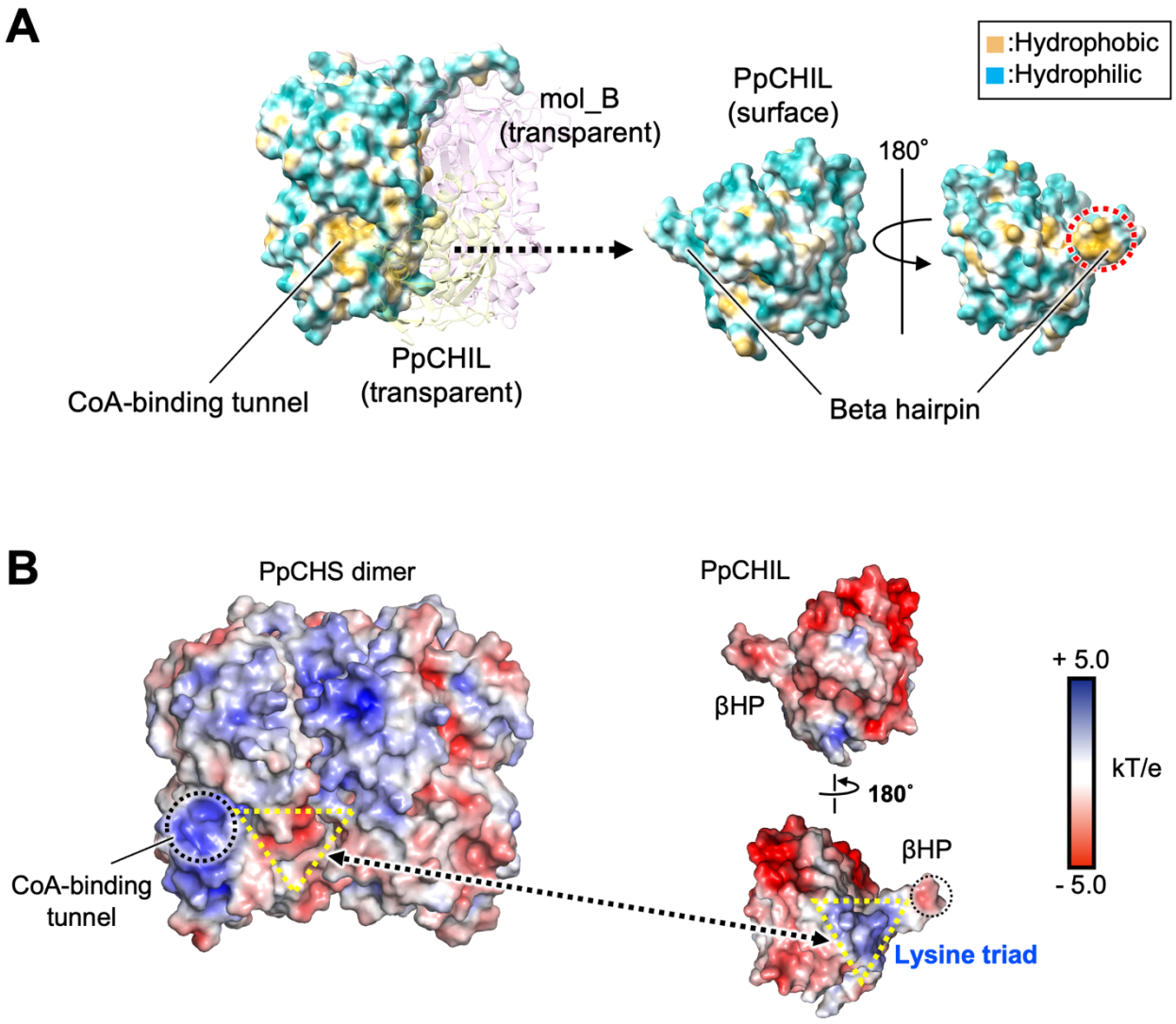

Supplementary Fig. 4. Interactions involved in the formation of the PpCHS-CHIL complex. (A) Hydrophobic interactions between PpCHS and PpCHIL around the CoA-binding tunnel of PpCHS and βHP of PpCHIL. (B) Electrostatic surfaces of PpCHS and PpCHIL. Dotted circles (black) and triangles (yellow) on both protein molecules indicate putative pairs of interactions in the interface.

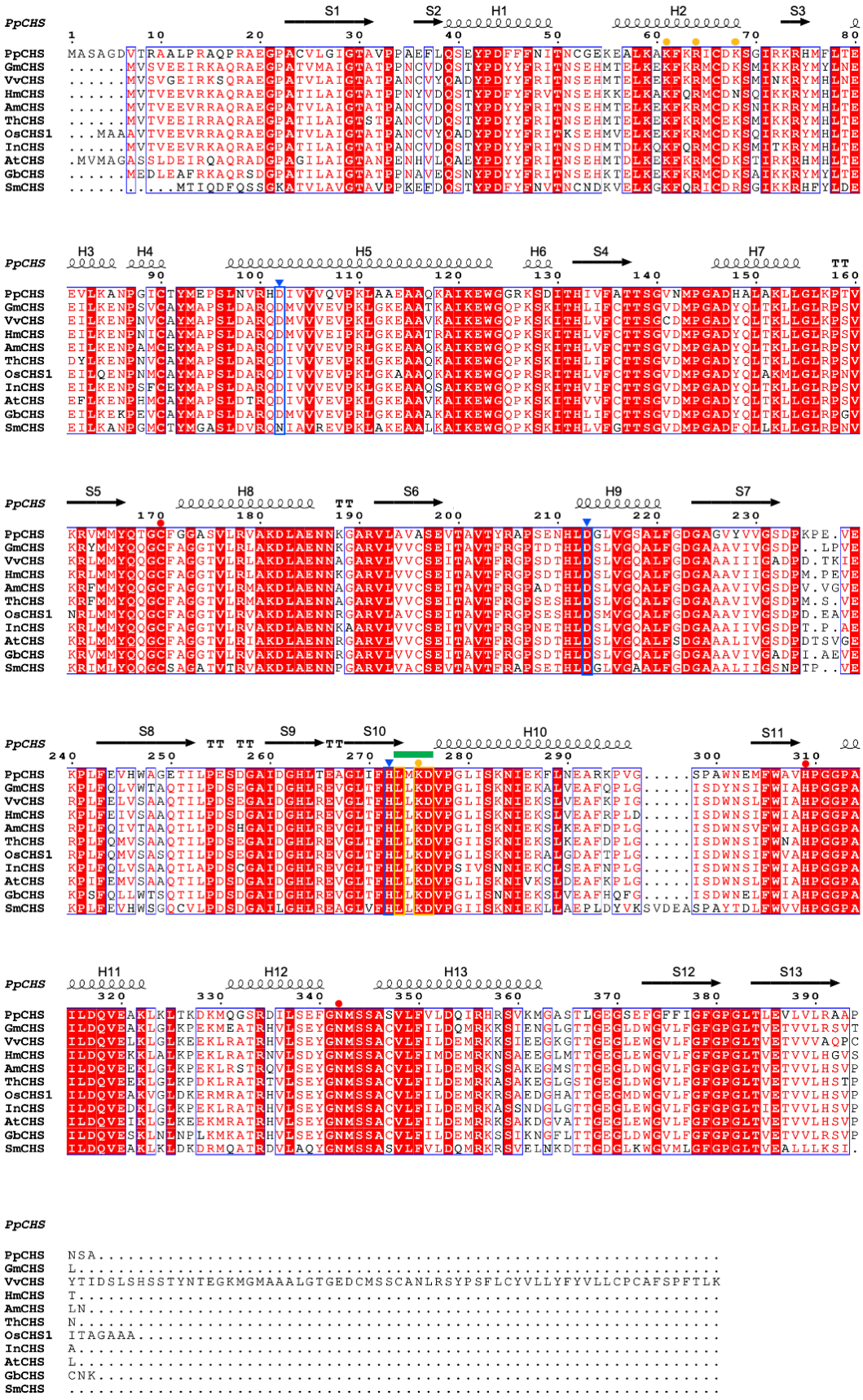

Supplementary Fig. 5 to be continued on the following page.

Supplementary Fig. S5. Amino acid sequence alignment of CHS proteins. CHS sequences from the following species are shown: *Glycine max* CHS1 (GmCHS, GenBank: X54644), *Vitis vinifera* (VvCHS, Phytozome v12.1: GSVIVT01032968001), *Hydrangea macrophylla* (HmCHS, GenBank: AB011467), *Antirrhinum majus* (AmCHS, GenBank: X03710), *Torenia* hybrid cultivar (ThCHS, GenBank: AB012923), *Oryza sativa* CHS1 (OsCHS, Phytozome v12.1: LOC_Os11g32650), *Ipomoea nil* CHS-D (InCHS, GenBank: AB001818), *Arabidopsis thaliana* CHS (TRANSPARENT TESTA 4; AtCHS, Phytozome v12.1: AT5G13930), *Ginkgo biloba* (GbCHS, GenBank: AY647263), and *Selaginella moellendorffii* (SmCHS, Phytozome v12.1: 270496). Secondary structural elements of PpCHS are shown and labeled above the sequence. Strict β-turns are indicated as TT. Red columns with white letters highlight residues identical to those in PpCHS; white columns with red letters indicate similar residues. Blue triangles mark residues in PpCHS (Asp102^{PpCHS}, Asp213^{PpCHS}, and His272^{PpCHS}) that interact via polar interactions with the lysine triad of PpCHIL. A thick green line indicates the K-loop (Leu273^{PpCHS}–Asp276^{PpCHS}). Orange circles mark residues involved in CoA binding in the PpCHS–CoA complex (Lys61^{PpCHS}, Arg64^{PpCHS}, Lys68^{PpCHS}, and Lys275^{PpCHS}). Red circles indicate putative catalytic residues (Cys170^{PpCHS} and Asn342^{PpCHS}).

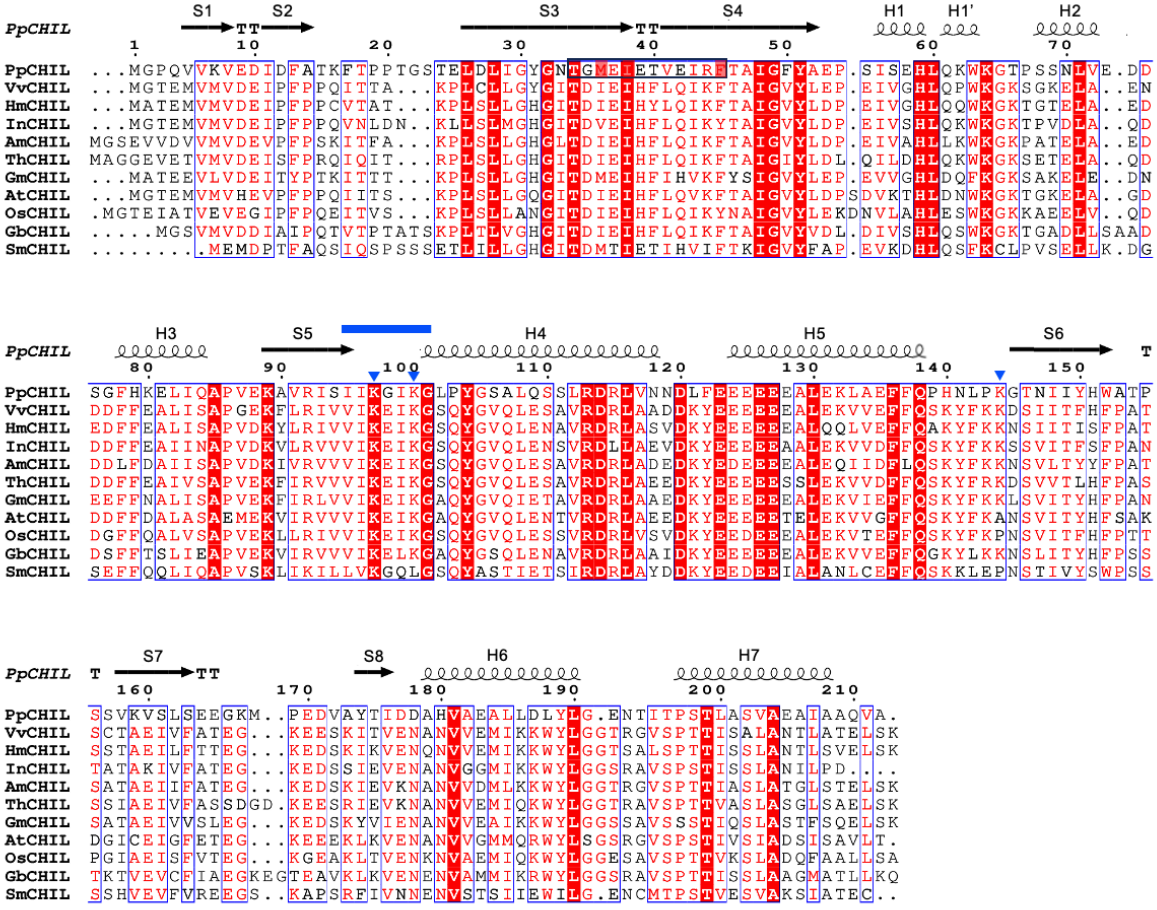

Supplementary Fig. 6. Amino acid sequence alignment of CHIL proteins. CHIL sequences from the following species are included: *Physcomitrella patens* (PpCHIL (PpCHIL-B)), *Vitis vinifera* (VvCHIL), *Hydrangea macrophylla* (HmCHIL), *Ipomoea nil* (InCHIL), *Antirrhinum majus* (AmCHIL), *Torenia* hybrid cultivar (ThCHIL (ThCHIL-A)), *Glycine max* (GmCHIL), *Arabidopsis thaliana* (AtCHIL), *Oryza sativa* (OsCHIL (OsCHIL-A)), *Ginkgo biloba* (GbCHIL), and *Selaginella moellendorffii* (SmCHIL). Secondary structural elements of PpCHIL are indicated above the alignment. H and S denote α-helices and β-strands, respectively; H1′ indicates a 3_{10}-helix; and strict β-turns are labeled as TT. Red columns with white letters highlight residues identical to those in PpCHIL; white columns with red letters indicate similar residues. The βHP region of PpCHIL is boxed. Blue triangles mark the lysine triad (Lys97^{PpCHIL}, Lys100^{PpCHIL}, and Lys144^{PpCHIL}) involved in polar interactions with PpCHS. A thick blue line above the sequence marks the loop region containing two highly conserved Lys residues (Lys97^{PpCHIL} and Lys100^{PpCHIL}). For CHIL sequence accession numbers, see reference[11].

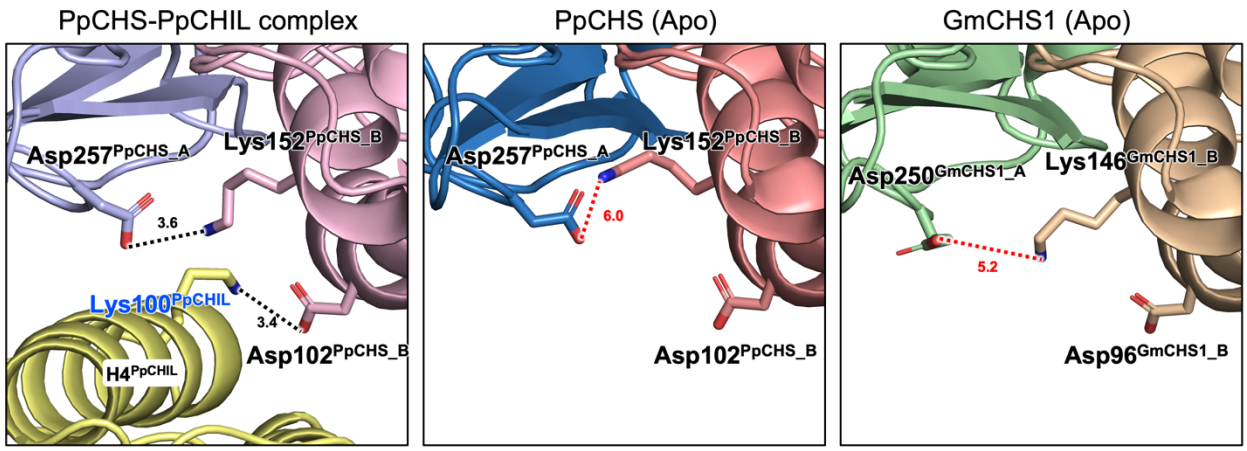

Supplementary Fig. 7. Formation of inter-subunit salt bridge between Asp257^{PpCHS_A} and Lys152^{PpCHS_B} in PpCHS–PpCHIL. There are no polar interactions in the corresponding positions of apo PpCHS (center panel) and apo GmCHS1 (right panel, PDB: 7BUR).

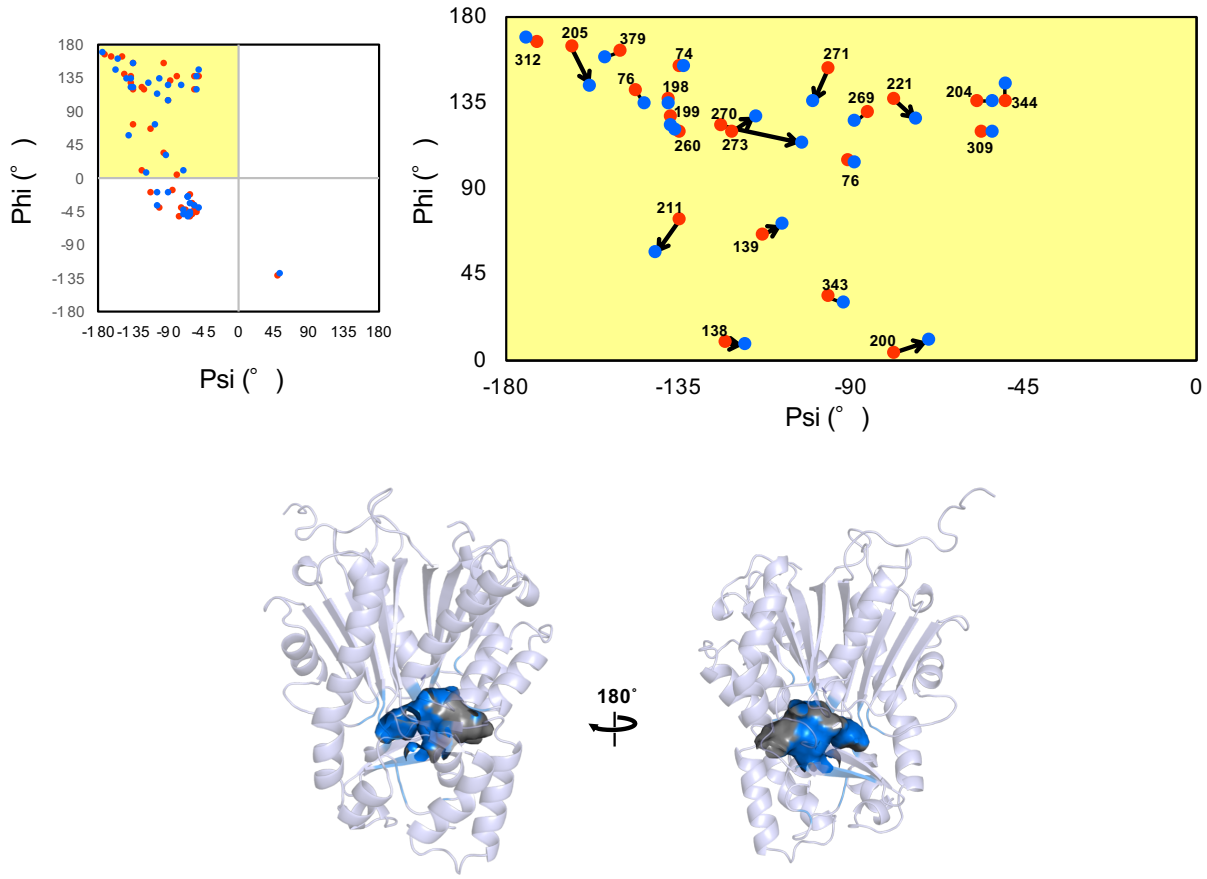

Supplementary Fig. 8. Structural changes in the active-site cavity. Top panels: Ramachandran plots for active-site cavity residues (blue: PpCHS–PpCHIL; red: PpCHS–CoA). An enlarged view of a specific region from the top-left Ramachandran plot is shown in the right panel. Bottom panel: The residues corresponding to the enlarged region (top right panel) are highlighted in blue on a surface representation of the active-site cavity.

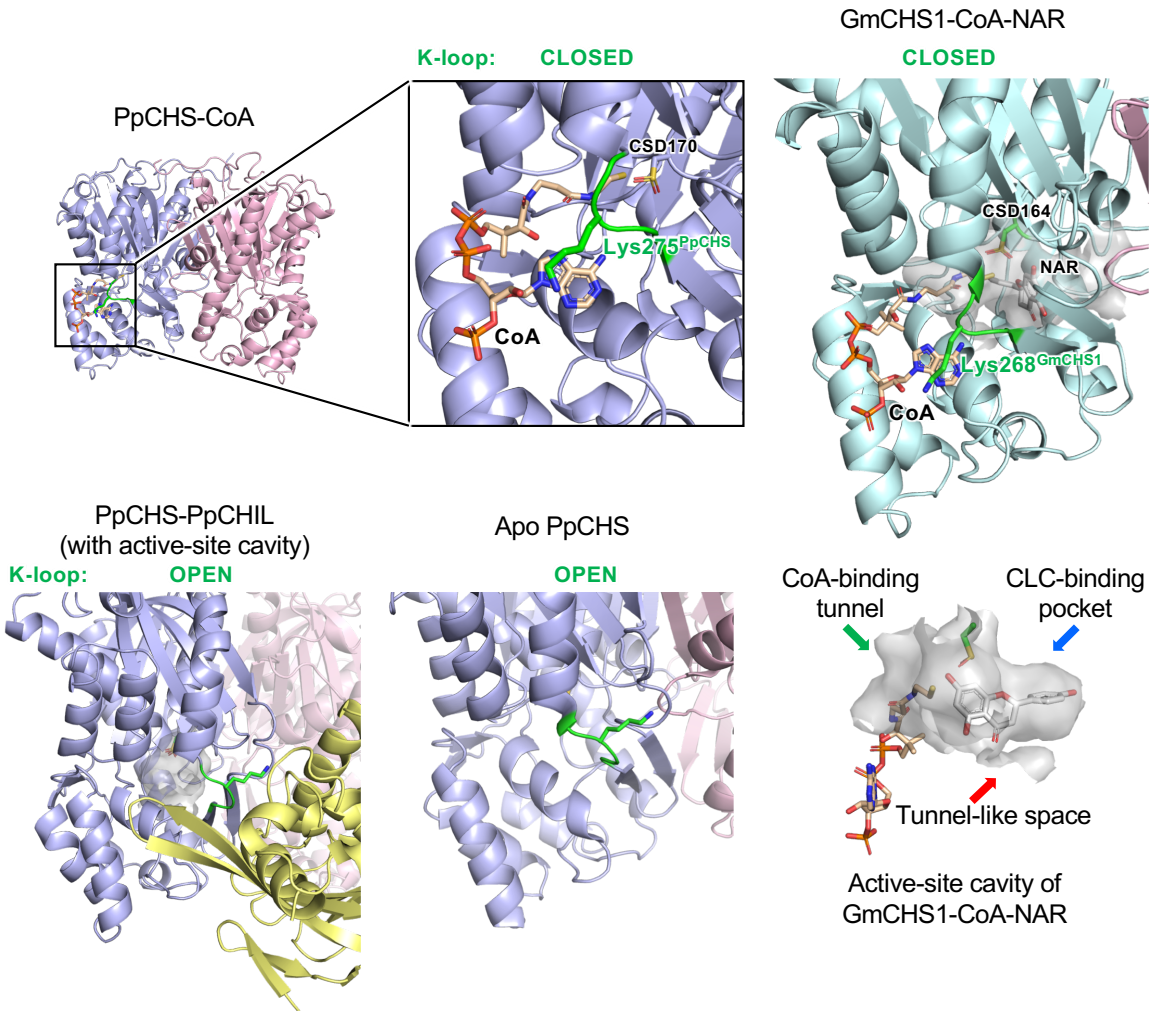

Supplementary Fig. 9. Comparison of K-loop conformations across various CHS structures. The K-loop with Lys275 (sticks) is colored green. Top panels: Crystal structures of PpCHS–CoA (left and center) and GmCHS1–CoA–Naringenin (NAR) (right, PDB: 8JRD) are compared. The active-site cavity is presented as a gray surface on the right panel. Bound CoA and NAR molecules are presented as sticks. Bottom panels: Structures of PpCHS–PpCHIL with its active-site cavity (left) and apo PpCHS (center, PDB: 6DX7). Right: Active-site cavity (gray surface representation) of GmCHS1–CoA–NAR viewed from a different perspective than the top right panel. Arrows indicate the CoA-binding tunnel, CLC-binding pocket, and a tunnel-like space.

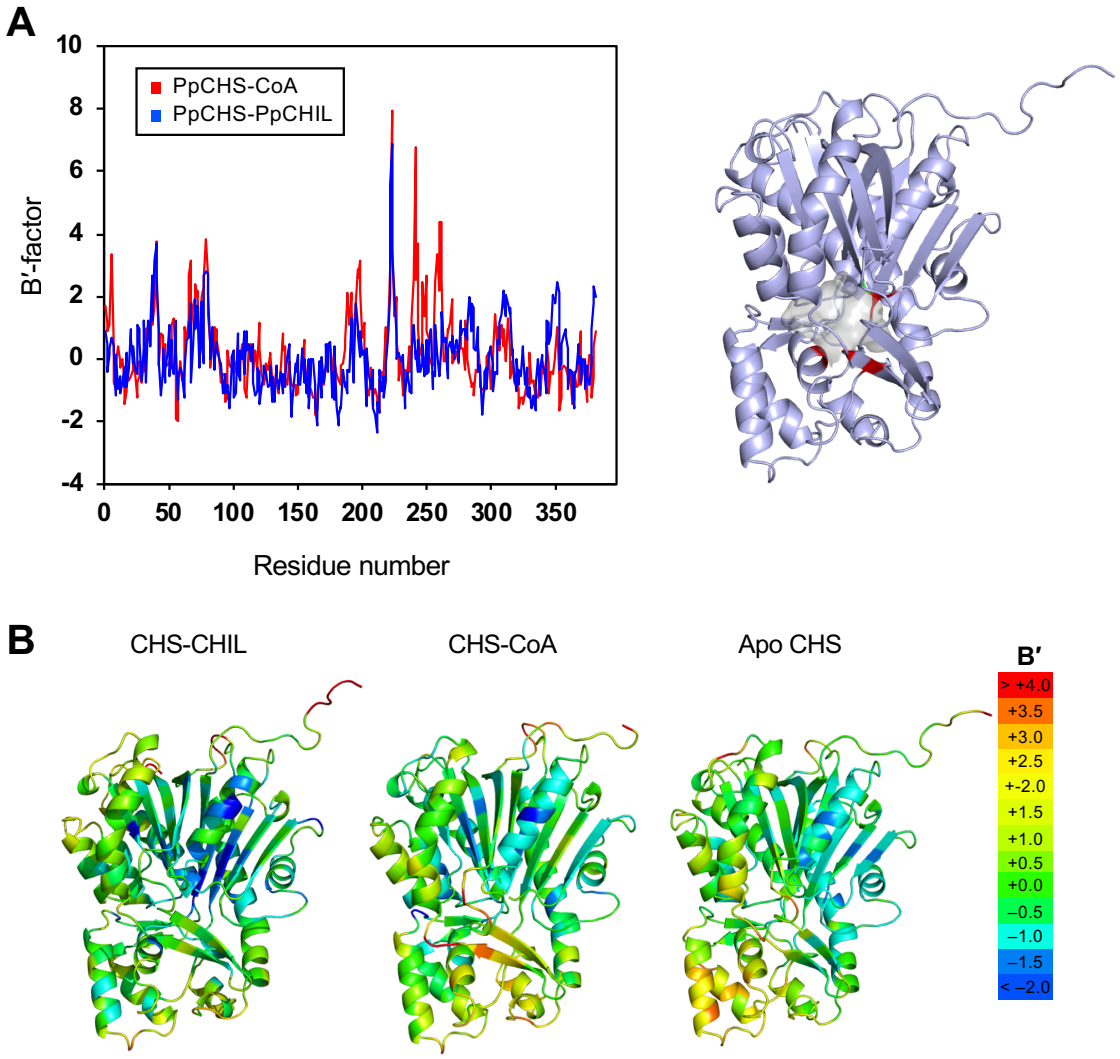

Supplementary Fig. 10. CoA binding enhances the mobility of both the K-loop and the surrounding CLC-binding pocket in CHS.
(A) Left: Normalized B-factor (B′-factor) profiles comparing PpCHS-CoA (red) and PpCHS-PpCHIL (blue) structures. Right: Monomeric PpCHS-CoA structure with the active-site cavity shown as a transparent surface. Residues with elevated B′-factors in the vicinity of the CLC-binding pocket are colored red. (B) B′-factor heat maps of PpCHS in the PpCHS–PpCHIL (left), PpCHS–CoA (center), and apo PpCHS (right) states.

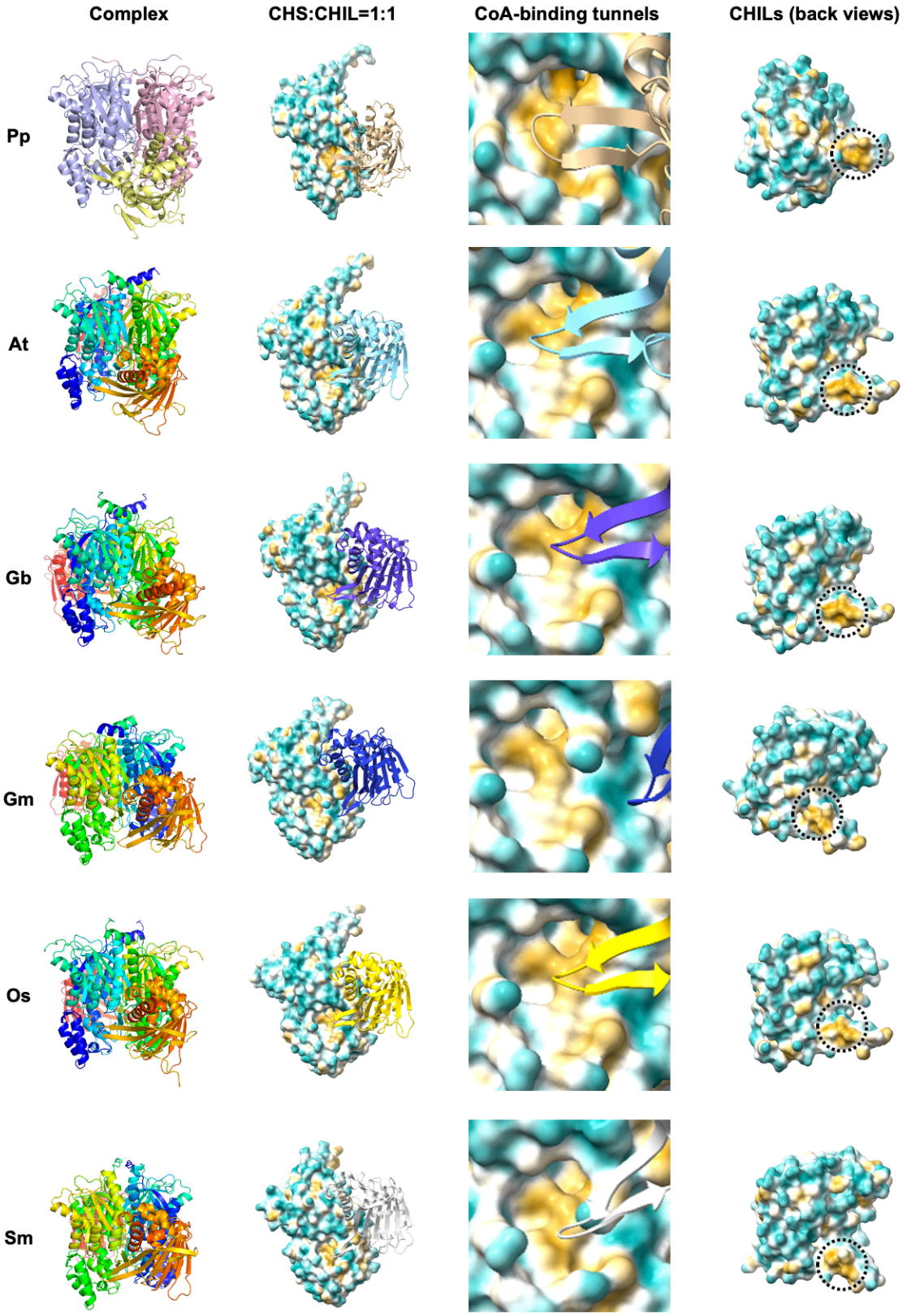

Supplementary Fig. 11 to be continued on the following page.

Supplementary Fig. 11. Computational docking study of the CHS-CHIL complex. Calculated CHS and CHIL complex structures in various land plants. Topological relationships between CHSs and CHILs in the complexes are similar among land plants, whereas the hydrophobic properties of CoA-binding tunnels (colored as shown in fig. S4A) and βHP positions vary. Dotted circles on the right indicate hydrophobic patches in βHPs of CHILs approaching CHSs. Pp: *Physcomitrella patens*; At: *Arabidopsis thaliana*; Gb: *Ginkgo biloba*; Gm: *Glycine max*; Os: *Oryza sativa*; Sm: *Selaginella moellendorffii*.

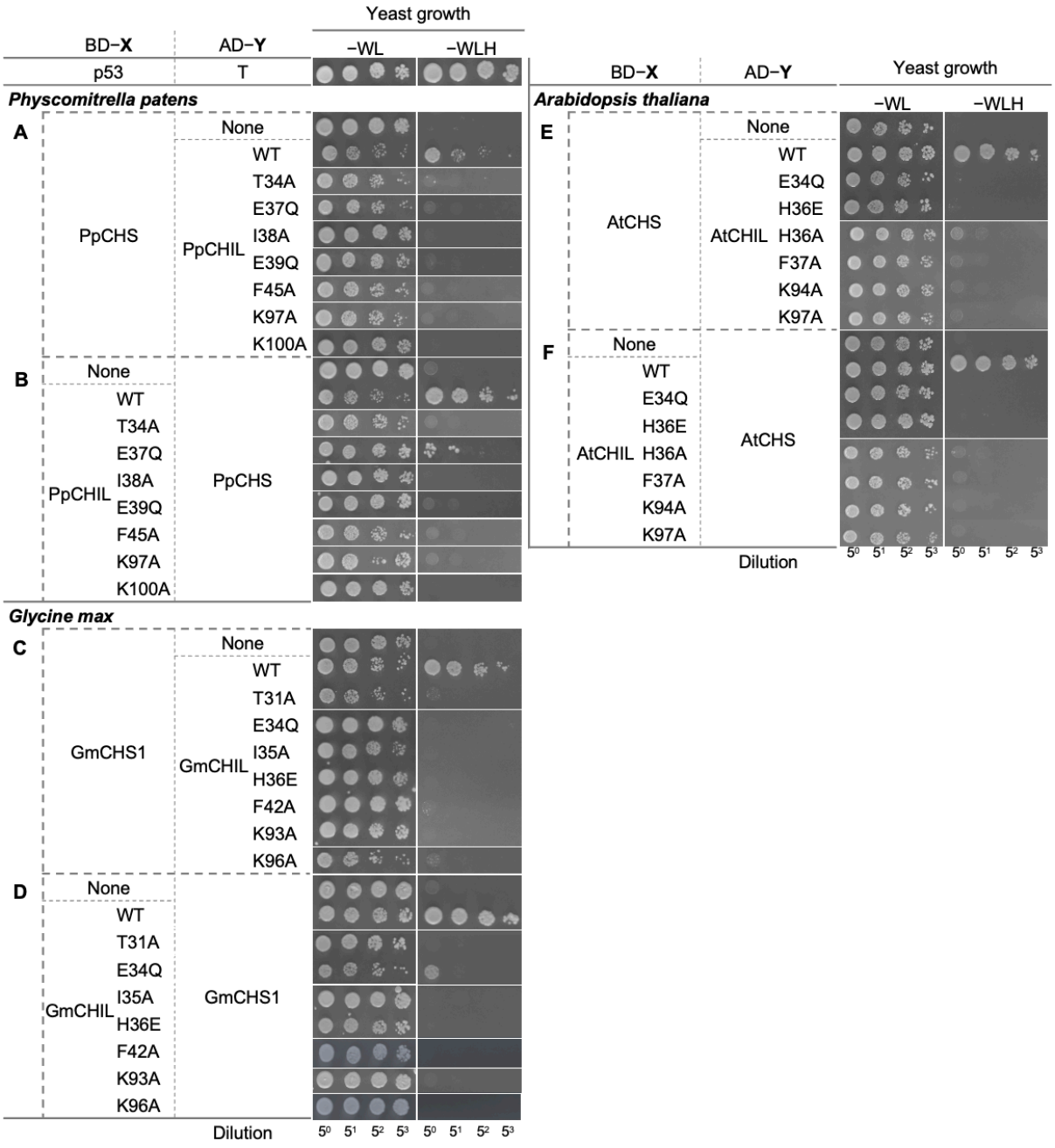

Supplementary Fig. 12. Mutational analysis of CHIL–CHS interactions in *Physcomitrella patens* (A, B), *Glycine max* (C, D), and *Arabidopsis thaliana* (E, F). Binary interactions between CHIL (wild-type and mutants) and CHS were analyzed using a GAL4-based yeast two-hybrid system[30]. Yeast cells co-expressing CHIL and CHS fused to the activation domain (AD; AD-Y columns) or DNA-binding domain (BD; BD-X columns) of GAL4 were spotted onto selective media. Growth on –WLH medium (lacking tryptophan, leucine, and histidine) indicates a positive interaction. (A, B) BD- or AD-tagged PpCHS was co-expressed with AD- or BD-tagged PpCHIL or its mutants; "None" indicates AD or BD alone. (C, D) BD-GmCHS1 or AD-GmCHS1 was co-expressed with AD- or BD-tagged GmCHIL or its mutants. (E, F) BD-AtCHS or AD-AtCHS was co-expressed with AD- or BD-tagged AtCHIL or its mutants. For each condition, 5 μL of a 5-fold serial dilution of yeast suspension was spotted onto synthetic dropout agar plates: –WL (lacking tryptophan and leucine) and –WLH.

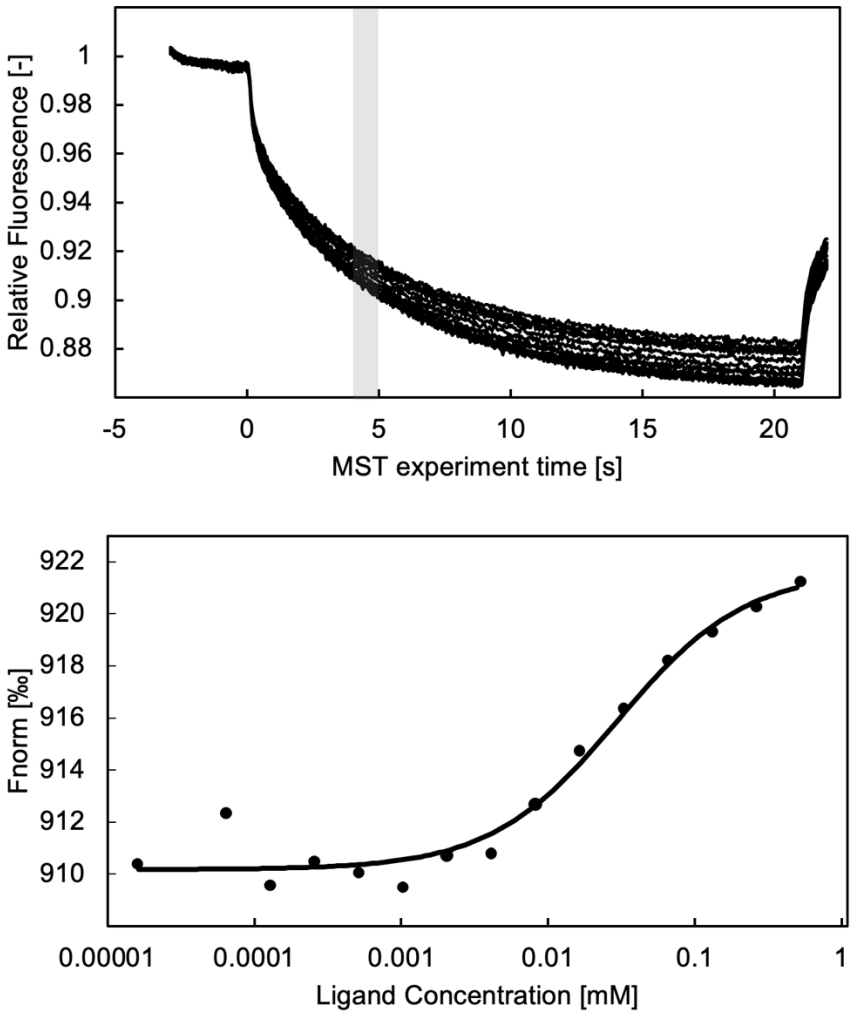

Supplementary Fig. 13. Interaction between PpCHS and PpCHIL according to a microscale thermophoresis analysis. Upper panel: The interaction between PpCHIL and PpCHS was monitored using fluorescent molecular signals labeled on PpCHS. The fluorescent signal traces of PpCHIL titration are shown. Lower panel: Fitting of the change in the fluorescence signal (F_{norm}) using the Hill equation is shown. Fluorescent signal changes during the time indicated by a gray rectangle (upper panel) were used for calculations.

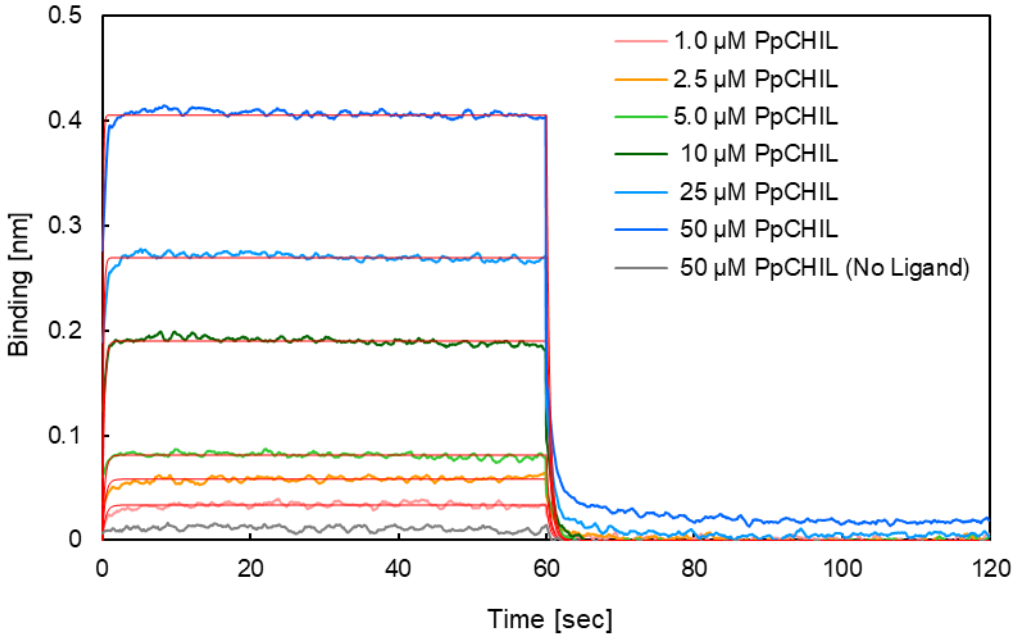

Supplementary Fig. 14. Biolayer interferometry analysis of interaction between PpCHS and PpCHIL. Binding of His_6-PpCHIL to immobilized biotinylated His_6-Avi-PpCHS was analyzed by biolayer interferometry using the Octet R2 system. Streptavidin biosensors were loaded with biotinylated PpCHS, followed by incubation with increasing concentrations of His_6-PpCHIL (1.0 to 50 μM). Sensorgrams show the association phase (0–60 s) and dissociation phase (60–120 s). Control data obtained using biosensors without immobilized PpCHS (50 μM PpCHIL, gray) are shown as the negative control.

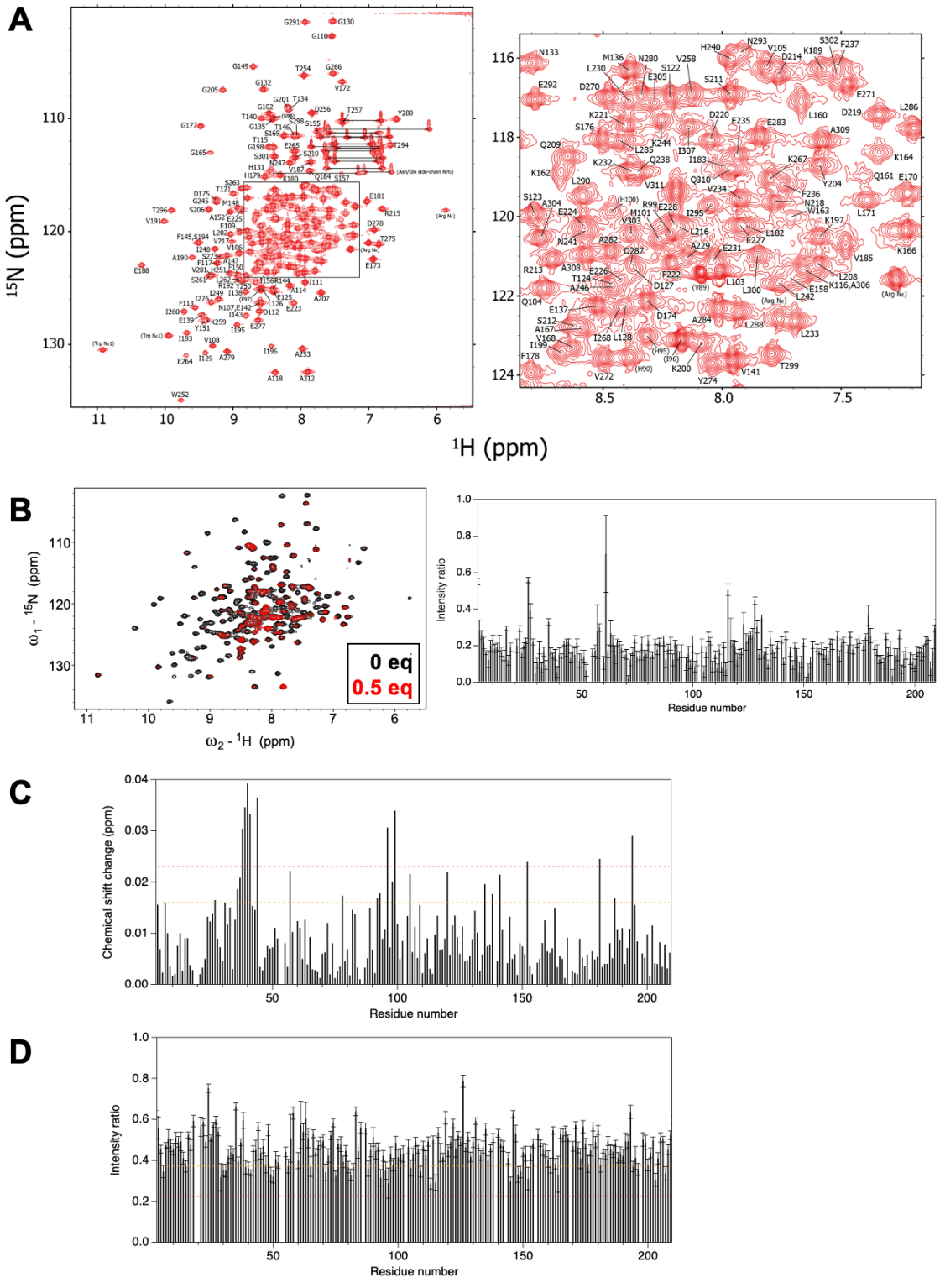

Supplementary Fig. 15. NMR analysis of the interaction between PpCHS and PpCHIL. (**A**) Left panel: ^{1}H-^{15}N HSQC spectra of ^{13}C- and ^{15}N-labeled PpCHIL. Right panel: Close-up view of the square in the left panel. The assigned amino acid residues (one-letter notation) of PpCHIL are

Supplementary Fig. 15 to be continued on the following page.

labeled. (**B**) ^{1}H-^{15}N HSQC spectra of ^{15}N-labeled PpCHIL in the absence (black) and presence (red) of 0.5 equivalents of PpCHS under 0 mM NaCl conditions. Fold-changes of signal intensities after the titration of PpCHS is shown on the right. (**C**) Chemical shift changes in the titration experiment involving PpCHS under 50 mM NaCl conditions. The cutoffs of the chemical shift perturbation mapping in Fig. 3C are shown as a dotted orange line ($\Delta\delta_{ave} + \Delta\delta_{SD}$) and a dotted red line ($\Delta\delta_{ave} + 2\Delta\delta_{SD}$), where $\Delta\delta_{ave}$ and $\Delta\delta_{SD}$ are the average and standard deviation, respectively, of the chemical shift change following the addition of the ligand. (**D**) Fold-changes of signal intensities (I) in the titration experiment shown in Fig. 3C. Dotted lines represent $(I_{0.5eq}/I_{0eq})_{ave} + (I_{0.5eq}/I_{0eq})_{SD}$ (orange) and $(I_{0.5eq}/I_{0eq})_{ave} + 2(I_{0.5eq}/I_{0eq})_{SD}$ (red) of the intensity ratio in this experiment.

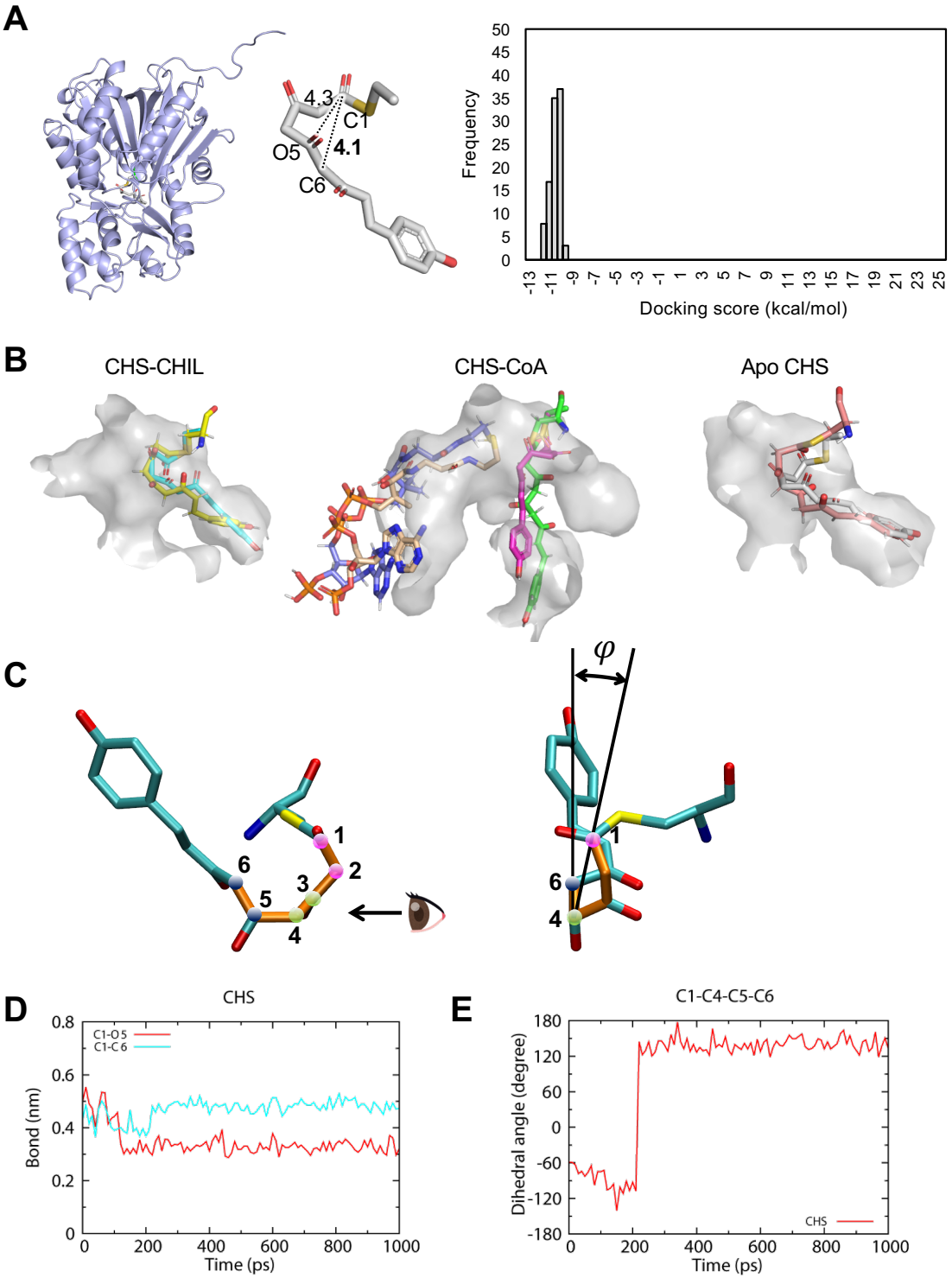

Supplementary Fig. 16. Computational simulations of T-i conformational dynamics. (A) Conformation of covalently bound T-i (center) and its associated docking scores (right) from covalent docking with apo PpCHS (PDB: 6DX7). (E) Comparison of initial and final T-i

conformations from 1,000-ps MD simulations of PpCHS. Initial T-i models are colored as in Fig. 4AB and Fig. S16A. Final T-i conformations are depicted with hydrogens (left: yellow-based stick; center: green-based stick; right: pink-based stick). The initial CoA model is colored as in Fig. 2B, with the final model shown as a blue-based stick with hydrogens. (C) Schematic illustration of dihedral angle (φ) analysis. T-i carbon atoms (C1-C6) are shown as spheres, colored as in Fig. 1. The right-hand T-i view corresponds to the perspective indicated by the eye in the left diagram. A 0° angle (φ) indicates optimal conditions for C6–C1 Claisen cyclization. (D) Time-dependent changes in the C6–C1 (blue) and O5–C1 (red) distances during a 1,000-ps molecular dynamics (MD) simulation of apo PpCHS. (E) Dihedral angle analysis of T-i carbon atoms (C1-C4-C5-C6) in apo PpCHS.

Supplementary Tables

Supplementary Table 1. Data and refinement statistics for crystal structures

	PpCHS-PpCHIL	PpCHIL	PpCHS-CoA
Data collection			
Space group	*P1*	*C2*	*P21212*
Cell dimensions			
a, b, c (Å)	79.9, 88.9, 118.0	61.5, 45.9, 76.3	190.2, 199.0, 68.4
α, β, γ (°)	74.4, 74.3, 68.8	90, 113.2, 90	90, 90, 90
Resolution (Å)*	50.0-1.92 (2.04-1.92)	50.0-1.87 (1.98 - 1.87)	50.0 - 2.64 (2.80 - 2.64)
Observed reflections	624,785 (102,663)	277,448 (41,842)	892,976 (137,670)
Unique reflections	216,275 (34,942)	16,352 (2,546)	76,561 (12,150)
†R_{meas} (R_{rim})	0.17 (1.13)	0.45 (6.02)	0.39 (1.80)
$<I/\sigma(I)>$	5.16 (1.01)	10.8 (1.15)	7.82 (1.75)
$CC_{1/2}$ (%)	98.6 (61.0)	99.7 (58.2)	96.8 (53.5)
Completeness (%)	98.9 (99.1)	99.8 (99.9)	99.0 (98.7)
Redundancy	2.89 (2.94)	17.0 (16.4)	11.7 (11.3)
Refinement			
Resolution (Å)	43.4-1.92	35.5-1.87	48.13 – 2.64
R_{factor} /R_{free}	0.17 / 0.21	0.19 / 0.23	0.20 / 0.24
Number of atoms			
Protein	18,347	1,633	17,518
Ligand/ion	26	21	208
Water	2,644	136	323
Average B factors			
Protein	34.6	25.3	34.0
Ligand/ion	51.2	54.1	45.6
Water	42.6	34.1	27.2
Rmsds bond length/bond angle			
Bond length (Å)	0.007	0.006	0.012
Bond angle (°)	0.963	0.823	1.345
Ramachandran plot			
Most favored (%)	97.7	99.5	97.4
Additionally allowed (%)	2.3	0.5	2.6
PDB entry	9KAH	9KAI	9KAJ

*Values in parentheses are for the highest resolution shell.
†$R_{meas} = R_{rim} = \Sigma_{hkl}(N/N-1)^{1/2}\Sigma_i|I_i(hkl) - <I(hkl)>| / \Sigma_{hkl}\Sigma_i I_i(hkl)$

Supplementary Table 2. Kinetic and thermodynamic parameters of PpCHS–PpCHIL interaction

Method	k_{on} ($s^{-1}M^{-1}$)	k_{off} (s^{-1})	K_d (μM)
MST*			31.8 ± 1.5
BLI†	1.68×10^5	2.16	12.8 ± 0.7

* MST, Microscale thermophoresis. Buffer used for measurements was 20 mM HEPES-NaOH (pH 7.0) containing 150 mM NaCl and 0.1% (w/v) Tween 20.

† BLI, Biolayer interferometry. Buffer used for measurements was 100 mM HEPES-KOH (pH 7.5) containing 0.1% (w/v) bovine serum albumin.

Supplementary Table 3. Kinetic parameters of PpCHS-catalyzed THC production

CHIL	k_{cat} (s^{-1})	K_m (μM)	k_{cat}/K_m (s^{-1} M^{-1})
For *p*-coumaroyl-CoA*			
–	$2.63\times10^{-3} \pm 8.5\times10^{-5}$	3.80 ± 0.59	6.9×10^{2}
+	$6.40\times10^{-2} \pm 6.5\times10^{-3}$	25.9 ± 5.5	2.5×10^{3}
For malonyl-CoA†			
–	$3.45\times10^{-3} \pm 3.1\times10^{-4}$	1.46 ± 0.86	2.4×10^{2}
+	$6.84\times10^{-2} \pm 3.3\times10^{-3}$	18.4 ± 2.8	3.7×10^{3}

* 100 μM malonyl-CoA was used as the extender substrate.
† 50 μM *p*-coumaroyl-CoA was used as the starter substrate.

Supplementary Table 4. List of oligonucleotide primers used in this study

Mutant	Primer name	Sequence (5′→3′) *
PpCHIL		
	CDS-f	TGATCTCAGAGGAGGACCTGCATATGGGTCTCCAAGTTGTG
	CDS-r	TGCGGCCGCTGCAGGTCGACGGATCCTCATGCAACCTGGGCAG
T34A	T34A-f	ATGGCAACGCGGGAATGGAGATTGAG
	T34A-r	CATTCCCGCGTTGCCATGGCCG
E37Q	E37Q-f	CAGATTGAGACTGTGGAAATCAGGTTTA
	E37Q-r	CATTCCCGTGTTGCCATG
I38A	I38A-f	TCGGCCATGGCAACACGGGAATGGAGGCTGAGACTGT GGAAATCAGGTTTAC
	I38A-r	TCCCGTGTTGCCATGGCCG
E39Q	E39Q-f	CAGACTGTGGAAATCAGGTTTACTGC
	E39Q-r	AATCTCCATTCCCGTGTTGC
F45A	F45A-f	AATCAGGGCTACTGCCATGGGCTTCTAC
	F45A-r	ATGGCAGTAGCCCTGATTTCCACAGTCTCAATC
K97A	K97A-f	CATCATCGCAGGGATCAAGGGCCTC
	K97A-r	GATCCCTGCGATGATGGAGATTCGCAC
K100A	K100A-f	TCTCCATCATCAAAGGGATCGCTGGCCTCCCCTATGGC
	K100A-r	GATCCCTTTGATGATGGAG
GmCHIL		
	CDS-f	CTCAGAGGAGGACCTGCATATGGCTACTGAAGAGGTTTTG
	CDS-r	GCTGCAGGTCGACGGATCCTCACTTGGACAACTCCTGC
T31A	T31A-f	CTTTGCTTGGCCATGGAATCGCCGACATGGAGATTCACTTCATC
	T31A-r	GATGAAGTGAATCTCCATGTCGGCGATTCCATGGCCAAGCAAAG
E34Q	E34Q-f	CATGGAATCACCGACATGCAGATTCACTTCATCCATGTGAAATTC
	E34Q-r	GAATTTCACATGGATGAAGTGAATCTGCATGTCGGTGATTCCATG
I35A	I35A-f	GGAATCACCGACATGGAGGCTCACTTCATCCATGTGAAATTC
	I35A-r	GAATTTCACATGGATGAAGTGAGCCTCCATGTCGGTGATTCC
H36E	H36E-f	GAATCACCGACATGGAGATTGAGTTCATCCATGTGAAATTCTATTC
	H36E-r	GAATAGAATTTCACATGGATGAACTCAATCTCCATGTCGGTGATTC
F42A	F42A-f	GATTCACTTCATCCATGTGAAAGCCTATTCAATCGGGGTTTATTTG
	F42A-r	CAAATAAACCCCGATTGAATAGGCTTTCACATGGATGAAGTGAATC
K93A	K93A-f	GAAGTTTATTAGACTTGTGGTGATCGCAGAGATCAAGGGTGCACAG
	K93A-r	CTGTGCACCCTTGATCTCTGCGATCACCACAAGTCTAATAAACTTC
K96A	K96A-f	CTTGTGGTGATCAAAGAGATCGCGGGTGCACAGTATGGGGTTC
	K96A-r	GAACCCCATACTGTGCACCCGCGATCTCTTTGATCACCACAAG
AtCHIL		
	CDS-f	CTCAGAGGAGGACCTGCATATGGGAACAGAGATGGTCATG
	CDS-r	GCTGCAGGTCGACGGATCCTTAGGTTAAAACTGCGGAGATTG
E34Q	E34Q-f	GCCAAGGGATCACAGACATTCAAATCCACTTTCTTCAAGTGAAG
	E34Q-r	AATGTCTGTGATCCCTTGG
H36E	H36E-f	GCCAAGGGATCACAGACATTGAGATCGAATTTCTTCA AGTGAAGTTCACTG
	H36E-r	AATGTCTGTGATCCCTTGG
H36A	H36A-f	TTGAGATCGCCTTTCTTCAAGTGAAGTTCACTG
	H36A-r	TGAAGAAAGGCGATCTCAATGTCTGTGATCCC
F37A	F37A-f	GAGATCCACGCTCTTCAAGTGAAGTTCACTGC
	F37A-r	CTTGAAGAGCGTGGATCTCAATGTCTGTGATC
K94A	K94A-f	GTGGTGATAGCGGAGATAAAAGGAGCTCAGTACG
	K94A-r	TTTATCTCCGCTATCACCACCACTCTTATAACCTTC
K97A	K97A-f	AGGAGATAGCAGGAGCTCAGTACGGAGTG
	K97A-r	TGAGCTCCTGCTATCTCCTTTATCACCACCACTC

* Underlining shows the mutation site.

Supplementary Notes

Supplementary Note 1

Our previous BLI measurements of CHS–CHIL interactions in various land plants, including *P. patens*, yielded K_d values ranging from 3 to 126 nM (*11*), which are substantially lower than those obtained in the present study. Upon investigation, we found that these earlier values could at least in part be explained by non-specific binding of the analyte protein (glutathione *S*-transferase–tagged CHIL) to the His_6-CHS-immobilized biosensor. To resolve this issue, we refined the BLI assay system by immobilizing biotinylated His_6–Avi–PpCHS onto a streptavidin-coated biosensor, using His_6-tagged CHIL as the analyte, and including 0.1% (w/v) bovine serum albumin in the assay buffer to suppress non-specific interactions. The K_d value obtained using this improved BLI setup was consistent with those derived from MST analysis and the SEC results in the presence of 200 mM NaCl.

Supplementary Note 2

A 1-μs MD simulation of the Ti-bound PpCHS–PpCHIL complex revealed that the complex undergoes a transition from a tightly associated "closed" state, as seen in the crystal structure, to a more relaxed "open" state, characterized by a wider gap between the two proteins. This closed-to-open transition of the two proteins occurs near the βHP region, and the βHP becomes slightly more remote from PpCHS in the open conformation.